Dalton Transactions

Accepted Manuscript

ROYAL SOCIETY OF CHEMISTRY

www.rsc.org/dalton

Synthesis, DNA binding, cellular DNA lesion and cytotoxicity of a series of new benzimidazole-based Schiff base copper(II) complexes

Anup Paul,[a]* Sellamuthu Anbu,[a] Gunjan Sharma,[b] Maxim L. Kuznetsov,[a] Biplob Koch,[b]* M.Fátima C. Guedes da Silva,[a]* Armando J. L. Pombeiro[a]*

The synthesis, characterization and biological evaluation of a series of new benzimidazole-based Schiff base copper(II) complexes are described. One of the compounds has a higher cytotoxic effect than cisplatin on lung cancer (A-549) cell line.

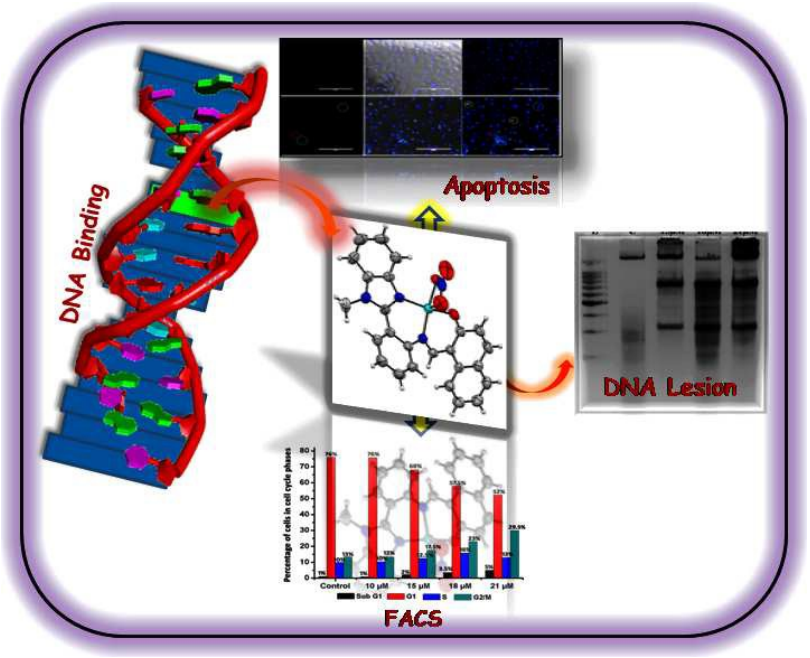

Synthesis, DNA binding, cellular DNA lesion and cytotoxicity of a series of new benzimidazole-based Schiff base copper(II) complexes

Anup Paul,[a]* Sellamuthu Anbu,[a] Gunjan Sharma,[b] Maxim L. Kuznetsov,[a] Biplob Koch,[b]* M. Fátima C. Guedes da Silva,[a]* Armando J. L. Pombeiro[a]*

[a]*Centro de Química Estrutural, Instituto Superior Técnico, Universidade de Lisboa, Av. Rovisco Pais, 1049-001 Lisboa. Portugal.*

[b]*Departments of Zoology, Faculty of Science, Banaras Hindu University, Varanasi - 221 005 (U.P.) India.*

Abstract

A series of new benzoimidazole containing compounds (2-(1-R-1-H-benzimidazol-2-yl)phenyl)imino)methyl) naphthol) **HL$^{1-3}$** (R = methyl, ethyl or propyl, respectively) has been synthesized by Schiff base condensation of 2-(1-R-1-H-benzo[d]imidazol-2-yl)aniline and 2-hydroxy-1-naphthaldehyde. The reactions of **HL$^{1-3}$** with $Cu(NO_3)_2.2.5H_2O$ led to the corresponding copper(II) complexes $[Cu(L)(NO_3)]$ **1**-**3**. All the compounds were characterized by conventional analytical techniques and, for **1** and **3**, also by single-crystal X-ray analysis. The interactions of complexes **1**-**3** with calf thymus DNA were studied by absorption and fluorescence spectroscopic techniques and the calculated binding constant (K_b) are in the range of 3.5×10^5 M^{-1} - 3.2×10^5 M^{-1}. Complexes **1**-**3** effectively bind DNA through intercalative mode, as proved by molecular docking studies. The binding affinity of the complexes decreases with the size increase in the N-alkyl substituent, in the order of **1** > **2** > **3,** which is also in accord with the calculated $LUMO_{complex}$ energies. They show substantial *in vitro* cytotoxic effect against human lung (A-549), breast (MDA-MB-231) and cervical (HeLa) cancer cell lines. Complex **1** exhibits a significant inhibitory effect on

proliferation of the A-549 cancer cells. The antiproliferative efficacy of **1** has also been analysed by DNA fragmentation assay, fluorescence activated cell sorting (FACS) and nuclear morphology using fluorescence microscope. The possible mode of apoptosis pathway of **1** has also been evaluated by reactive oxygen species (ROS) generation study.

***Corresponding authors.** E-mail: *kanupual@gmail.com*, *kochbiplob@gmail.com*, *fatima.guedes@tecnico.ulisboa.pt*, *pombeiro@tecnico.ulisboa.pt,*

Introduction

The majority of drugs used for cancer treatment are cytotoxic (cell-killing) interfering in some way with the operation of the DNA cells. The serendipitous discovery of cisplatin[1] has revolutionized the cancer treatment and many other platinum based drugs have been discovered.[2] However, side-effects associated with these drugs restrict their wider use.[3] Thus, in pursuit of overcoming these issues associated with Pt based anticancer drugs, non-platinum metal complexes are being explored, particularly those capable of binding DNA effectively.[4] Copper(II) complexes are regarded as promising and have attracted considerable attention owing to their capability of interacting directly with DNA/nuclear proteins.[5-7]

On the other hand, benzimidazole-based Schiff base metal complexes possess good antibacterial, antimalarial and antifungal activities.[8] Several 2-(2-aminophenyl)-1-*H*-benzimidazole derived qunizoline based metal complexes have been utilized as fluorescent probes for intracellular imaging.[9] Moreover, benzimidazole-based platinum complexes

have been extensively studied and the mechanism of cytotoxic properties has been discussed with regard to the development of new antitumor agents.[10]

However, benzimidazole-based Schiff base copper(II) complexes for DNA binding and cytotoxic properties are scarce.[11] Furthermore, the benzimidazole-based ligands are promising systems for the development of biologically active metal complexes, due to the structural similarity of the benzimidazole nucleus with natural compounds such as vitamin-B12 derivatives and purine bases. In particular, the non-planar nature of benzimidazole ligands, their flexibility and bulkiness affect the kinetics and cytotoxic properties of the corresponding metal complexes. In addition, benzimidazole-based ligands can possess hydroxyl and/or N-H moieties which can facilitate DNA cleavage in cancer cells.[12]

Thus, in light of our continuing investigation for developing new metal-based chemotherapeutic agents, we have designed a new series of N-alkyl substituted benzimidazole-based Schiff base copper(II) complexes [Cu(L)(NO_3)] and investigated their DNA interaction and *in vitro* cytotoxicity properties against human lung (A-549) cancer cell line. Furthermore, the action mechanism and apoptotic pathway of one of these complexes was investigated from the morphologic changes using fluorescence staining, fluorescence activated cell sorting (FACS), DNA fragmentation and by reactive oxygen species (ROS) generation studies.

Experimental Section

Materials and Physical methods

The reagents for the syntheses of the ligands and $Cu(NO_3)_2.2.5H_2O$ were obtained from commercial sources and used as received without further purifications. Solvents were dried and distilled prior to their use following standard procedures.[13] 3-(4,5-dimethylthiazol-2-yl)-2,5-diphenyltetrazolium bromide (MTT) and RPMI-1640 were purchased from Hi-Media, ethidium bromide (EB) from Acros Organics, Portugal. Calf Thymus (CT) DNA was purchased from Bangalore Genie (India). ^1H (300 MHz) and ^{13}C (75.45 MHz) NMR spectra were run on a Bruker 300 MHz spectrometer using tetramethylsilane [$Si(CH_3)_4$] as internal reference. IR and electronic absorption spectra were recorded on Bruker Alpha Fourier transform infrared (FT-IR) spectrometer and Perkin-Elmer LAMBDA 750 UV-visible spectrophotometer, respectively. Fluorescence emission studies were carried out on LS-55 fluorescence spectrometer (Perkin-Elmer, UK). The excitation and emission slit widths were set at 4.5 nm and the temperature was maintained by recycling water using a peltier system. Electrospray ionization mass spectrometric data (ESI-MS) were acquired in methanol on a Bruker Micro TOF QII, and THERMO Finnigan LCQ Advantage Max ion trap Mass Spectrometer.

Syntheses

Synthesis of 2-(1-methyl-1-*H*-benzo[d]imidazol-2-yl)aniline (P1)

To a solution of 2-(2-aminophenyl)-1-*H*-benzimidazole (209 mg, 1 mmol) in dry DMF (5 mL) sodium hydride (36 mg, 1.5 mmol; 60% dispersion in mineral oil, prewashed with hexane) was added in fractions, iodomethane (171 mg, 1.2 mmol) in dry DMF (5 mL) was added dropwise over 15 minutes and the reaction mixture stirred for 24 h. Completion of the reaction was monitored by TLC and, after filtration, the solvent was removed under

reduced pressure. The residue thus obtained was partitioned between ethyl acetate and water, the combined organic layers were washed with water, brine solution and dried over Na_2SO_4. Decantation followed by removal of the solvent under reduced pressure afforded the crude product which was further purified by silica gel column chromatography (EtOAc: Hexane; 1:9) to afford the desired product. Yield: 70% . Anal. Calcd. for $C_{14}H_{13}N_3$: C, 75.31; H, 5.87; N, 18.82 Found C, 75.41; H, 5.92; N, 18.72 %. ^{1}H NMR ($CDCl_3$, 300 MHz, δ ppm): 7.79 (s, Ar-H), 6.76-7.25 (m, Ar-H), 6.80 (d, J = 6.2, Ar-H), 3.83 (s, 3H, CH_3), 5.04 (s, 2H, NH_2). ^{13}C NMR ($CDCl_3$, 75.45 MHz, δ ppm): 155.21, 148.32, 145.10, 135.45, 130.34, 126.73, 122.14, 121.34, 120.52, 117.89, 112.32, 109.72, 31.27. ESI-MS in CH_3OH: Calcd. for $[(M + H)]^+$: m/z 224.1, found 224.0.

Synthesis of 2-(1-ethyl-1H-benzo[d]imidazol-2-yl)aniline (P2)

It was prepared following the above procedure for **P1** but using iodoethane (188 mg, 1.2 mmol) in place of iodomethane. Yield: 65%. Microanalytical data: $C_{15}H_{15}N_3$, Calcd. : C, 75.92; H, 6.37; N, 17.71%. Found C, 75.82; H, 6.28; N, 17.81%. ^{1}H NMR ($CDCl_3$, 300 MHz, δ ppm): 7.83 (s, Ar-H), 7.44-7.28 (m, Ar-H), 6.87 (d, J = 6.2, Ar-H), 5.06 (s, 2H, NH_2), 4.28 (q, 2H, -CH_2), 1.28 (t, 3H, -CH_3). ^{13}C NMR ($CDCl_3$, 75.45 MHz, δ ppm): 154.81, 148.62, 143.50, 136.45, 129.84, 125.13, 123.52, 120.75, 119.10, 118.91, 111.52, 109.82, 40.27. 16.21. ESI-MS in CH_3OH: Calcd. for $[(M + H)]^+$: m/z 238.1, found 238.0.

Synthesis of 2-(1-propyl-1-*H*-benzo[d]imidazol-2-yl)aniline (P3)

It was prepared following the above procedure for **P1** but using iodopropane (204 mg, 1.2 mmol) in place of iodomethane. Yield: 60%. Microanalytical data: $C_{16}H_{17}N_3$, Calcd. : C, 76.46; H, 6.82; N, 16.72%. Found C, 76.50; H, 6.78; N, 16.76%. ^{1}H NMR ($CDCl_3$, 300 MHz, δ

ppm): 7.82 (s, Ar-H), 7.44-7.28 (m, Ar-H), 6.87 (d, J = 6.2, Ar-H), 5.01 (s, 2H, NH_2), 4.19 (t, 2H, $-CH_2$), 3.2 (sep, 2H, $-CH_2$), 0.87 (t, 3H, $-CH_3$), ^{13}C NMR ($CDCl_3$, 75.45 MHz, δ ppm): 153.21, 146.36, 142.51, 134.25, 129.54, 126.33, 123.00, 119.84, 119.92, 116.27, 110.12, 109.12, 51.65, 24.34, 11.25. ESI-MS in CH_3OH: Calcd. for $[(M + H)]^+$: m/z 252.1, found 252.0.

Synthesis of 2-(1-methyl-1-*H*-benzimidazol-2-yl)phenyl)imino)methyl) naphthol (H L^1)

It was synthesized by following the general procedure described in the literature.[12*b*] To an ethanolic solution (50 mL) of **P1** (224 mg, 1 mmol), 2-hydroxy-1-naphthaldehyde dissolved in ethanol (5 ml, 122 mg, 1 mmol) and a catalytic amount of acetic acid were added and the reaction mixture refluxed for 5 h. After completion of the reaction (monitored by TLC), the volume of the reaction mixture was reduced to *ca.* 10 mL. Diethyl ether (5 mL) was added to it and the solution left undisturbed at -4 °C. After 4-5 days, light yellow needle shaped crystals appeared which were separated by filtration, washed with diethyl ether and dried in air. Yield: 75%. Microanalytical data: $C_{25}H_{19}N_30$, Calcd. : C, 79.55; H, 5.07; N, 11.13%. Found C, 79.80; H, 4.98; N, 10.98%. IR (KBr pellets, cm^{-1}): $\nu_{C=N}$: 1634. ^1H NMR ($CDCl_3$, 300 MHz, δ ppm): 14.43 (s, -OH), 9.41 (s, C(H)=N), 7.95 (d, J = 8.5 Hz, Ar-H), 7.88 (s, Ar-H), 7.78 (d, J = 9.1 Hz, Ar-H), 7.68 (m, Ar-H), 7.53 (s, Ar-H), 7.50 (s, Ar-H), 7.45 (s, Ar-H), 7.40 (s, Ar-H), 7.34 (m, Ar-H), 7.01 (d, J = 9.1 Hz, Ar-H), 3.71 (s, 3H, $-CH_3$). ^{13}C NMR ($CDCl_3$, 75.45 MHz, δ ppm): 166.30, 158.87, 136.15, 132.34, 131.48, 129.22, 128.07, 127.58, 126.65, 123.67, 123.02, 120.54, 119.84, 119.54, 119.17, 109.75, 30.95. ESI-MS in CH_3OH: Calcd. for $[(M + H)]^+$: m/z 378.44, found 379.0.

Synthesis of 2-(1-ethyl-1-*H*-benzimidazol-2-yl)phenyl)imino)methyl)phenol (HL^2)

It was prepared following the above procedure for **HL^1** but using **P2** (238 mg, 1 mmol) and 2-hydroxy-1-naphthaldehyde (122 mg, 1 mmol). Yield: 60%. Microanalytical data: $C_{26}H_{21}N_30$, Calcd. : C, 79.77; H, 5.41; N, 10.73%. Found C, 79.89; H, 5.50; N, 10.79%. IR (KBr pellets, cm^{-1}): $\nu_{C=N}$: 1618. ^1H NMR ($CDCl_3$, 300 MHz, δ ppm): 14.37 (s, -OH), 9.42 (s, C(H)=N), 7.94 (d, J = 8.5 Hz, Ar-H), 7.87 (s, Ar-H), 7.76 (d, J = 9.1 Hz, Ar-H), 7.68 (m, Ar-H), 7.54 (s, Ar-H), 7.50 (s, Ar-H), 7.43(s, Ar-H), 7.39 (s, Ar-H), 7.34 (m, Ar-H), 6.97 (d, J = 9.1 Hz, Ar-H), 4.18 (q, 2H, $-CH_2$), 1.29 (t, 3H, $-CH_3$). ^{13}C NMR ($CDCl_3$, 75.45 MHz, δ ppm): 164.78, 159.10, 151. 83, 146.85, 136.09, 132.91, 131.77, 129.18, 128.06, 127.56, 126.61, 123.65, 123.65, 119.71, 119.27, 110.18, 107.04, 106.74, 39.34, 14.99. ESI-MS in CH_3OH: Calcd. for $[(M + H)]^+$: m/z 392.46, found 392.89.

Synthesis of 2-(1-propyl-1-*H*-benzimidazol-2-yl)phenyl)imino)methyl)phenol (HL^3)

It was prepared following the above procedure for **HL^1** but using **P3** (406 mg, 1 mmol) and 2-hydroxy-1-naphthaldehyde (122 mg, 1 mmol). Yield: 40%. Microanalytical data: $C_{27}H_{23}N_30$, Calcd. : C, 79.97; H, 5.72; N, 10.36%. Found C, 79.88; H, 5.67; N, 10.48%. IR (KBr pellets, cm^{-1}): $\nu_{C=N}$: 1614. ^1H NMR ($CDCl_3$, 300 MHz, δ ppm): 14.38 (s, -OH), 9.40 (s, C(H)=N), 7.91 (d, J = 8.5 Hz, Ar-H), 7.88 (s, Ar-H), 7.75 (d, J = 9.1 Hz, Ar-H), 7.65 (m, Ar-H), 7.53 (s, Ar-H), 7.49 (s, Ar-H), 7.43 (d, J = 9.1 Hz, Ar-H), 7.37 (s, Ar-H), 7.32 (m, Ar-H), 6.96 (d, J = 9.1 Hz, Ar-H), 4.13 (q, 2H, $-CH_2$), 1.71 (sep, 2H, $-CH_2$), 0.74 (t, 3H, $-CH_3$). ^{13}C NMR ($CDCl_3$, 75.45 MHz, δ ppm): 165.76, 158.82, 151.57, 146.83, 143.23, 131.35, 129.18, 128.02, 123.61, 122.61, 122.30, 120.47, 119.95, 119.55, 110.32, 109.20, 46.08, 22.78, 11.23. ESI-MS in CH_3OH: Calcd. for $[(M + H)]^+$: m/z 406.49, found 407.0.

Synthesis of [Cu(L^1)(NO_3)] (1)

A methanolic solution (2 mL) of $CuNO_3 \cdot 2.5H_2O$ (32 mg, 0.13 mmol) was slowly layered upon a chloroform solution of **HL^1** (50 mg, 0.13 mmol) and left undisturbed. After 3-4 days an olive-green microcrystalline product deposited which was separated by filtration, washed with diethyl ether and dried at room temperature. Yield: 45%. Microanalytical data: $C_{25}H_{18}CuN_4O_4$, Calcd. : C, 59.82; H, 3.61; N, 11.16%. Found C, 60.02; H, 3.69; N, 11.29%. IR (KBr pellet, cm^{-1}): ν 1614 (C=N), 1471_{vs} (N-O), 1246s (N-O). ESI-MS in CH_3OH: Calcd. for $[CuL^1]^+$: m/z 439.1, found 439.0. $\lambda_{max,}$ nm (ε, M^{-1} cm^{-1}) in DMF: 327 (0.9×10^4), 426 (0.6×10^4).

Synthesis of [Cu(L^2)(NO_3)] (2)

$CuNO_3 \cdot 2.5H_2O$ (30 mg, 0.13 mmol) dissolved in methanol (2 mL) was added dropwise to a methanolic solution (2 mL) of **HL^2** (50 mg, 0.13 mmol) and the reaction mixture stirred for 1 h at room temperature. The resulting solution was filtered and left for slow evaporation. After a few days, an olive-green microcrystalline product deposited and was separated by filtration, washed with diethyl ether and dried at room temperature. Yield: 50%. Microanalytical data: $C_{26}H_{20}CuN_4O_4$, Calcd. : C, 60.52; H, 3.91; N, 10.86 %. Found C, 60.58; H, 4.01; N, 10.95%. IR (KBr pellet, cm^{-1}): ν 1614 (C=N), 1471_{vs} (N-O), 1246s (N-O). ESI-MS in CH_3OH: Calcd. for $[CuL^2]^+$: m/z 453.0, found 453.1. $\lambda_{max,}$ nm (ε, M^{-1} cm^{-1}) in DMF: 330 (1.5×10^4), 426 (1.1×10^4).

Synthesis of [Cu(L^3)(NO_3)] (3)

Compound **3** was prepared in an analogous procedure to that described for **1**, using $CuNO_3 \cdot 2.5H_2O$ (30 mg, 0.13 mmol) and **HL^3** (50 mg, 0.13 mmol). Yield: 40%.

Microanalytical data: $C_{27}H_{22}CuN_4O_4$, Calcd. : C, 61.18; H, 4.18; N, 10.57%. Found C, 61.26; H, 4.11; N, 10.65%. (KBr pellets, cm^{-1}): ν 1614 (C=N), 1481_{vs} (N-O), 1246s (N-O). ESI-MS in CH_3OH: Calcd. for $[CuL^3]^+$: m/z 467.1, found 467.1. $\lambda_{max,}$ nm (ε, M^{-1} cm^{-1}) in DMF: 332 (2.1×10^4), 430 (1.4×10^4).

X-ray Structure Determination

Crystals of **1** and **3** suitable for single crystal X-ray analyses were obtained from slow evaporation of methanol-chloroform or methanol solutions of the compounds. The crystals were mounted in nylon loops and measured at 296 K. Intensity data were collected using a Bruker APEX-II PHOTON 100 diffractometer with graphite monochromated Mo Kα (λ = 0.71069 nm) radiation. Data were collected using phi and omega scans of 0.5° per frame and a full sphere of data was obtained. Cell parameters were retrieved using Bruker SMART[15a] software and refined using Bruker SAINT[14a] on all the observed reflections. Absorption corrections were applied using SADABS.[14a] Structure was solved by direct methods by using SIR97 software[14b] and refined with SHELXL-2013.[14c] Calculations were performed using the WinGX System-Version 1.80.03.[14d] All non-hydrogen atoms were refined anisotropically. The hydrogen atoms bonded to carbon atoms were included in the model at geometrically calculated positions and refined using a riding model. U_{iso}(H) were defined as $1.2U_{eq}$ of the parent carbon atoms for phenyl and methylene residues and $1.5U_{eq}$ of the parent carbon atoms for the methyl groups. Crystallographic data and refinement parameters are summarized in Table 1 and a comparison of bond distances and angles are presented in Table 2. For compound **2** the very low quality of the structure prevents its discussion.

DNA Interaction Studies

Electronic absorption titration studies were carried out using a fixed concentration of compounds in DMF solution (1%) with increasing concentration of CT-DNA in 5 mM Tris HCl/50 mM NaCl buffer, pH 7.5, following an earlier procedure.[15] The purity of the CT-DNA was verified by electronic absorption studies following the ratio of absorbances at 260 and 280 nm, which was 1.9 and suggested that the DNA was sufficiently free of protein. The DNA concentration per nucleotide was determined by examining the molar extinction coefficient of 6600 M^{-1} cm^{-1} at 260 nm. An analogous method was used for emission studies also. EB displacement experiments were performed by monitoring the changes in fluorescence intensity at excitation (λ_{ex} = 525 nm) and emission (λ_{em} = 603 nm) wavelengths, after aliquot additions of compounds to the 5 mM Tris HCl/50 mM NaCl buffer, pH 7.5, of EB bounded DNA (EB-DNA).

DFT calculations and Molecular Docking

The full geometry optimization of complexes **1**–**3** has been carried out at the DFT level of theory using the M06-2X[16] functional with the help of the Gaussian-09 program package.[17] The relativistic Stuttgart pseudopotential that described 10 core electrons (MDF10) and the appropriate contracted basis set[18] were employed for the Cu atom while the standard basis set 6-31+G** was applied for all other atoms. No symmetry operations have been applied for any of the structures calculated. The Hessian matrix was calculated analytically for the optimized structures in order to prove the location of correct minima (no imaginary frequencies).

Molecular docking studies on **1-3** have been performed using HEX 8.0.0 software and visualization of the docked systems has been performed using Discovery Studio 3.5 software. The crystal structure of B-DNA (PDB ID: 1BNA) and human serum albumin (PDB ID: 1HA2) were obtained from the protein data bank (http://www.rcsb.org./pdb). The initial study of the DNA-complex interaction was carried out by docking of compounds **1**-**3** with DNA (PDB ID: 1BNA). For this, the whole DNA crystal structure was considered as active site to avoid biasness towards either DNA minor or major grooves during docking study. The parameters used for docking include: correlation type shape only, FFT mode 3D, grid dimension 0.6, receptor range 180, ligand range 180, twist range 360, distance range 40. The coordinates of complexes **1**-**3** were taken from DFT optimized structures, converted to the PDB format using Mercury software.

Cell Viability and Proliferation Assay/MTT Assays

Human lung carcinoma (A-549), cervical carcinoma (HeLa) and, breast adenocarcinoma (MDA-MB 231) cell lines were used to determine the anticancer and cytotoxic activity in this study. Cell viability was checked by MTT assay which is a colorimetric assay based on the conversion of the yellow tetrazolium salt MTT to purple formazan crystals after reaction with mitochondrial dehydrogenase of metabolically active cells.[19] Stock solutions of complexes **1**-**3** were prepared in DMSO and diluted with DMEM (Dulbecco's Modified Eagle's Medium) (the final concentration of DMSO did not exceeded 0.1% v/v). The cell lines were maintained in complete DMEM (culture medium consisting 10% fetal bovine serum, supplemented with 20 mM L-glutamine, 100 units/mL penicillin and 100 µg/mL streptomycin) at 37 °C in a humidified atmosphere of 5% CO_2. Briefly, $1x10^4$ lung A-549 or

HeLa or MDA-MB 231 cancer cells were seeded in three different 96 well cell culture plate. After 24 h, the culture medium was replaced by fresh medium containing various concentrations of **1-3** and incubated further for 24 h in a 5% CO_2 humidified atmosphere. The medium was then removed and 100 μL of fresh medium and 10 μL of 5 mg/mL MTT in phosphate buffered saline (PBS, pH 7.4) was added to each well for an additional 2 h. Finally, DMSO was added to dissolve the MTT formazan crystals followed by incubation for 30 mins. The absorbance of samples was measured at 570 nm with an ELISA plate reader. Cytotoxicity effect was revealed as the percentage of treated cells relative to untreated cells at A570 nm. Percent control was calculated using the following formula:

% Control = [Mean O. D. of Drug treated well / Mean O. D. of control well] × 100

Fluorescence staining of A-549 cells

Cells were seeded in 96 well plates and kept for 24 at 37 °C in a humidified atmosphere of 5% CO_2. After that, cells were treated with different concentration of complex **1** for 24 h. Subsequently, cells were washed with 1x PBS and stained with Hoechst 33342 (10μg/mL) and propidium iodide (5μg/mL) solution. Cells were then washed with PBS and images were taken in fluorescent microscope (Evos FL, Life technologies) in red and blue channel.

DNA fragmentation assay

DNA was isolated from control and treated A-549 cells according to the procedure described *by* Kuo *et al.*[20] Briefly, 1 × 10^5 lung cancer cells were seeded in 6 well plates and kept at 37 °C in a humidified atmosphere of 5% CO_2 and allowed to adhere overnight. Cells were incubated with different concentrations of complex **1** (15, 18 and 21 μM) for 24 h in DMEM with 10% FBS. After 24 h, cells were washed and lysed [20 mM Tris-Cl (pH-7.5),

0.15 M NaCl, 1 mM EDTA, 0.5% SDS] at 4 °C for 30 min and centrifuged (3,000 rpm for 10 min) at room temperature, the supernatant was collected, and 25 µL Proteinase K (stock 20 mg/mL) was added to it followed by incubation for 2 h at 37 °C. It was again centrifuged at 12,000 rpm for 30 min at 4^0C and supernatant was collected in another tube, DNA was precipitated by addition of chilled absolute ethanol and 0.1 M NaCl. It was then collected by centrifugation and washed thoroughly with 70% ethanol; the pellet was dried and dissolved in autoclaved double distilled water. DNA samples were prepared in a loading solution (0.25% bromophenol blue, 0.25% xylene cyanol FF and 30% glycerol) in 1:5 ratio and 10 µL of samples loaded in each well of 1.8% agarose gel containing 0.5 µg/mL ethidium bromide. Electrophoresis was carried out in TAE buffer for 2 h. The DNA bands in gel were photographed in a Gel documentation system (G: BOX, SYNGENE).

Cell cycle analysis

1×10^5 lung cancer cell lines were seeded in 6 well plates as described above, then treated with different concentrations of complex **1** for 24 h in DMEM with 10% FBS. Cells were then washed, trypsinised and fixed in ice cold 70% ethanol and kept overnight at -20 °C. Then the cells were washed twice in PBS, 500 μL of staining solution [960 μL of 0.1% (v/v) Triton x-100 solution, 20 μL of PI (1 mg/mL) solution and 20 μL of RNase (10 mg/mL in PBS)] were added in each sample and incubated for 30 min at room temperature in the dark. After the staining procedure, the samples were evaluated by a flow cytometer.

ROS generation assay

Intracellular reactive oxygen species level was assessed using DCFH-DA in an inverted fluorescence microscope. Briefly, A-549 cells were seeded in 96 well plates at a density of

$1x10^4$ cells per well and treated with different concentrations of complex **1** based on IC_{50} value for 24 h at 37 °C in a humidified atmosphere of 5% CO_2. The cells were then exposed to 10 µM of DCFH-DA solubilized in ethanol for 30 min. The samples were subjected to inverted fluorescence microscopy and DCF fluorescence was detected and photographed.

Results and Discussion

Synthesis and Characterization

Syntheses of **HL** [1], **HL**[2] and **HL**[3] has been achieved by condensation of N-alkyl substituted 2-aminophenylbenzimidazole (**P1**, **P2** and **P3**: Scheme S1, ESI) with 2-hydroxy-1-naphthaldehyde in a 1:1 molar ratio in ethanol with a catalytic amount of acetic acid under refluxing conditions (Scheme S2, ESI). Their ^1H and ^{13}C NMR spectra are detailed in the experimental section and relevant ones are presented in Figs. S1-S6, ESI. The mononuclear copper(II) complexes [Cu(L)(NO_3)] (**1**, L = L^1; **2**, L = L^2; **3**, L = L^3) were prepared by the reaction of the corresponding **HL**[1-3] with Cu(NO_3).2.5H_2O in a 1:1 molar ratio, in MeOH:$CHCl_3$ or MeOH, as depicted in Scheme 1.

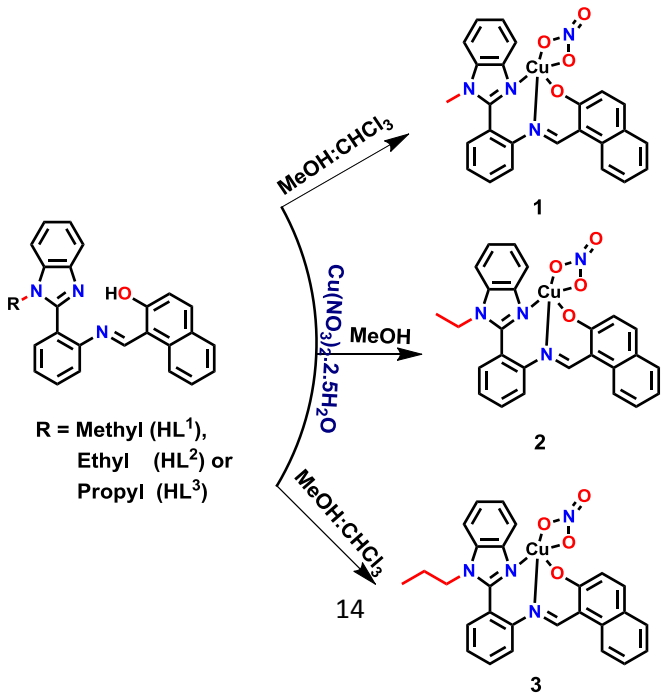

Scheme 1 Syntheses of complexes **1-3.**

These complexes are crystalline, non-hygroscopic solids, stable at room temperature, and soluble in MeOH, DMF, DMSO and partially soluble in water. They have been characterized by elemental analyses, FT-IR and ESI-MS spectral methods. The molecular structures of **1** and **3** have further been determined by single crystal X-ray crystallography.

The IR spectra of the free ligands **HL$^{1-3}$** clearly show ν(C=N) at *ca.* 1633, 1618, and 1614 cm^{-1}, respectively. In the complexes **1**-**3**, the *ν*(C=N) vibration is downshifted to a lower frequency by *ca.* 6-19 cm^{-1}, appearing at *ca.* 1614, 1612 and 1608 cm^{-1}, respectively. The presence of the coordinated nitrate is indicated by the bands observed for antisymmetric and symmetric stretching at *ca.* 1471-1481 and *ca*. 1246 cm^{-1}, respectively. The difference between the stretching N–O vibration bands (*ca.* 230 cm^{-1}) confirms the bidentate coordination of the nitrate ion.[21] The ESI mass spectra of **1-3** display the ion peaks at *m/z* 439.1, 453.1 and 467.1, respectively, assignable to the corresponding [ML]$^{+}$ ions (Figs. S7-S9, ESI).

The electronic absorption spectra of the complexes in DMF (experimental section) show peaks in the UV region at 327 (**1**), 330 (**2**) and 332 (**3**) nm which are attributed to $\pi \rightarrow \pi^{*}$ transitions of the coordinated ligands.[22] In addition, broad and strong bands observed at 426 nm (**1** and **2**) and 430 nm (**3**) are assigned to the ligand-to-metal charge transfer transition.[22]

Further, in order to monitor the stability of the complexes **1-3** in DMF and in DMSO solutions, UV/vis spectra were run for a period of 48 h. No changes were observed on the initial spectra of the solutions along that period, suggesting that the complexes under study are stable in both DMF and DMSO solutions (Fig. S10, ESI).

Crystal Structure

The single crystal X-ray diffraction studies of **1** and **3** indicate that they crystallize in the orthorhombic *P*bca and triclinic *P*-1 space groups, respectively. The molecular structures of **1** and **3** are shown in Figs. 1(a) and 1(b). The asymmetric units of the compounds consist of one (**1**) or two (**3**) independent complex molecules with the same coordination environment around the copper centres. In **3**, a significant difference is observed not only in the orientation of the propyl side groups but also in the angle between the least square planes of the two sets of fused rings in each molecule (51.38º and 56.61º for the Cu1 and Cu2 containing molecules, respectively). A superposition of the molecules showing this distinction is shown in Fig. S11, ESI. The copper(II) cation in **1** and **3** presents a N_2O_3 coordination environment which deviates from a regular square pyramid as a result of the μ_2-O-chelation of the nitrate anions [$\tau5$ = 0.10 (Cu1; in **1** and **3**) and 0.31 (Cu2 in **3**)].[23] Those dissimilar values of $\tau5$ in **3** may be associated with the steric influence from propyl groups, the highest value concerning the molecule where this moiety is nearly in the plane of its benzimidazole group. The metals are involved in two fused 6-membered CuC_3NO and CuC_3N_2 metallacycles. While the former is roughly planar with the metal cation at a distance of 0.360 (**1**) or 0.376 and 0.031 Å (**3**; Cu1 and Cu2, in this order) from the least-square plane defined by the non-metal atoms, the latter adopts a boat conformation.

The Cu-N bond distances range from 1.926(6) to 1.980(6) Å, while the Cu-O lengths involving the organic ligand assume values of 1.862(5) or 1.868(5) Å. This distance is significantly shorter than those involving the nitrate anion (values between 1.990(6) and 2.497(7) Å).

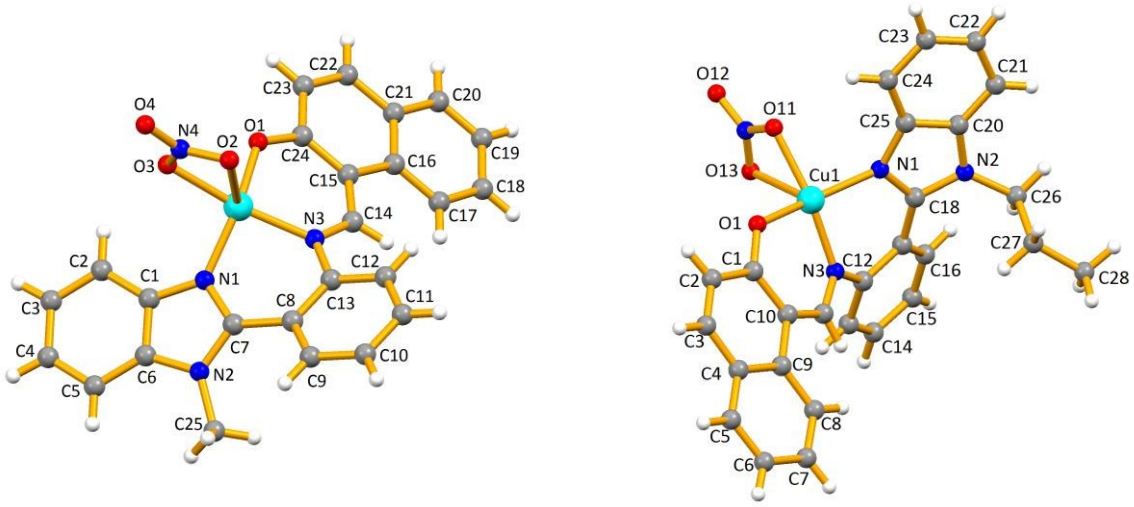

(a) **(b)**

Fig. 1. X-ray molecular structures of compounds **1** and **3** with atom numbering scheme. For **3**, only one of the complex molecules is shown.

On the other hand, because of the difficulty in obtaining high-quality crystals of compound **2**, despite repeated attempts, the quality of the X-ray results for **2** is less than optimal, and thus prevented its discussion. However, it appears to be sufficient to indicate that the compound **2** also possesses a N_2O_3 coordination environment as that of **1** and **3**, with a distorted square pyramidal geometry. A representation of the structure of **2** and unit cell parameters are given in Fig. S12, ESI.

DNA interaction studies

Electronic absorption titration

DNA is an important cellular target of many metallodrugs for the treatment of multiple pathologies, including cancer, and plays a relevant role in unrevealing the potential of metal binding sites with either electron rich nucleobases or phosphate oxygen atoms of the DNA duplex.[24] Thus the binding ability of the complexes **1-3** with CT DNA is characterized by measuring the effects on UV spectroscopy. Absorption spectroscopic titration experiments of the complexes **1-3** (1.7×10^{-5} M) in 5 mM TrisHCl/50 mM NaCl buffer at pH 7.5, were performed using a fixed metal concentration to which increasing amounts of the DNA stock solution (0-12 μM) was gradually added. The binding of the complexes to duplex DNA led to a decrease in the absorption intensities with a slight red shift in the absorption spectra (Fig. 2 and Figs S13-14, ESI). To compare quantitatively the affinity of the complexes towards DNA, the binding constant (K_b) of each complexes to CT DNA was determined by monitoring the changes of absorbance at 327, 328 and 330 nm, respectively, with increasing concentration of DNA.

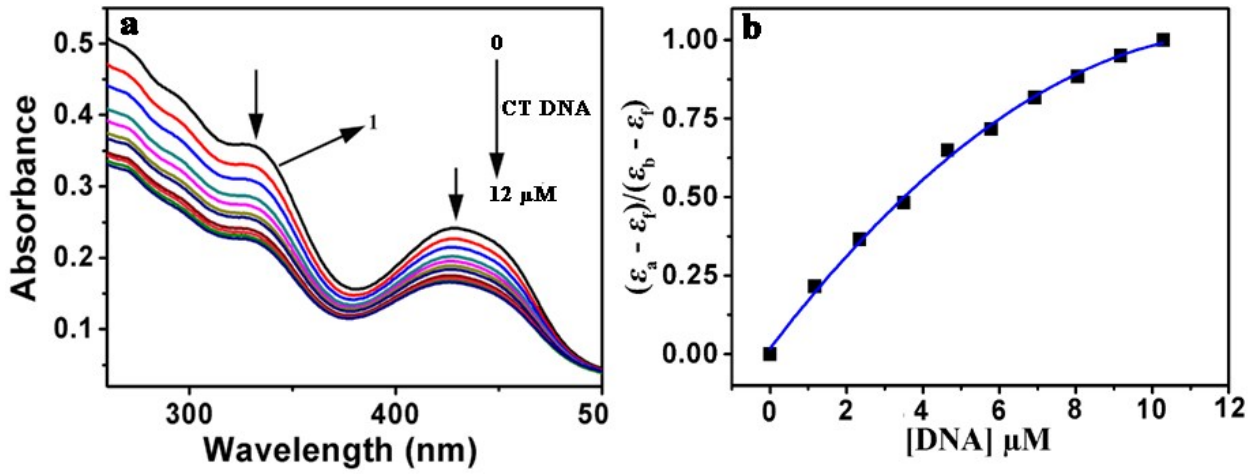

Fig. 2. (a) Absorption spectra of complex **1** (1.7×10^{-5} M) in the absence and presence of increasing amounts of CT-DNA (0–12 μM) at 25 °C in 5 mM Tris-HCl/50 mM NaCl buffer

(pH 7.5). Arrow shows the absorbance changing upon increasing DNA concentrations. (b) The non-linear fit of $(\varepsilon_a - \varepsilon_f)/(\varepsilon_b - \varepsilon_f)$ *vs.* [DNA].

The absorption titration profiles of **1**-**3** clearly suggest intercalation between these complexes and DNA, because in general intercalation is associated to hypochromism with red-shifts, involving a stacking interaction between the aromatic chromophore of complexes and the base pairs of DNA.[25] Further, on the basis of the hypochromism effect in the complexes, we can also ascertain that their modes of interaction are similar.

Further, to evaluate the binding strength of the complexes with CT DNA, the equilibrium binding constants (K_b) and binding site size (s, per base pair) were determined from a non-linear fit of the plot of $(\varepsilon_a - \varepsilon_f)/(\varepsilon_b - \varepsilon_f)$ *vs.* [DNA] applying the McGhee-von Hippel (MvH) method and using the expression of Bard and coworkers[26] (equation 1):

$$(\varepsilon_a - \varepsilon_f)/(\varepsilon_b - \varepsilon_f) = (b - (b^2 - 2K_b^2C_t[\mathrm{DNA}]_t/s)^{½})/2K_bC_t \quad (1)$$

where, $b = 1 + K_bC_t + K_b[\mathrm{DNA}]/2s$,

K_b is the binding constant, C_t is the total concentration of the metal complex, and s is the fitting constant giving an estimate of the binding site size (in base pairs) of the metal complex interacting with the DNA, ε_f, ε_a and ε_b are, respectively, the molar extinction coefficients of the free complex in solution, complex bound to DNA at a definite concentration and the complex in completely bound form with CT DNA.

The calculated intrinsic equilibrium binding constant (K_b) of complexes **1**-**3** were found to be 3.45(±0.23) × 10^5 M^{-1} (s = 0.43), 3.33 (±0.18) × 10^5 M^{-1} (s = 0.35) and 3.15 (±0.16) × 10^5 M^{-1} (s = 0.33), respectively, and are comparable to those of earlier reported copper(II)

complexes.[22,27,28] These values found for our complexes, although higher, are of the same order of magnitude of the classical intercalator EB[29] (K_b = 1.23 (s = 0.07) 10^5 M^{-1}), which further suggests the binding of the complexes to DNA through an intercalative mode. This intercalation ability of the complexes **1**-**3** can be associated to the presence of the naphthalene moiety in the ligand.[30] Further, the relatively stronger binding affinity of complex **1** compared to those of **2** and **3** can be due to the presence of the least bulky N-alkyl moiety in the ligand framework, the binding affinity progressively decreasing with the size increase in the N-alkyl substituent, in the order of **1** > **2** > **3**.

Ethidium Bromide (EB) Displacement Assays

Further to substantiate the effective mode of binding of the complexes **1**-**3** to DNA, *via* the EB displacement technique,[31] competitive binding studies have been performed for those complexes using EB bound to DNA (EB-DNA) in 5 mM Tris-HCl/50 mM NaCl buffer at pH 7.5. The emission spectra of EB and EB-DNA in absence and presence of the complexes (0-30 μM) are shown in Fig. 3a, and Figs. S15-S16, ESI. The addition of complex **1**-**3** (0- 30 μM) to EB-DNA (λ_{em} = 603 nm) leads to quenching of the emission intensity by 82, 77 and 68%, respectively relative to the initial fluorescence intensity. A steady decrease in the emission intensity of EB-DNA, upon addition of complexes **1**-**3**, suggests displacement of the EB, which is the characteristic feature of intercalators. Further, quenching strength (K_q) of complexes towards EB-DNA has been calculated using Stern-Volmer equation shown below (equation 2):

$$F^0/F = K_q\,[Q] + 1 \qquad (2)$$

where, F^0 and F correspond to the fluorescence intensities in the absence and presence of complexes, respectively, and [Q] represents the ratio of total concentration of complexes to that of CT-DNA. K_q is a linear Stern–Volmer quenching constant, which can be obtained from the linear regression of F^0/F with [Q]. The calculated K_q values for the complexes **1**-**3** are 3.3×10^5, 2.8×10^5 and 1.8×10^5, respectively.

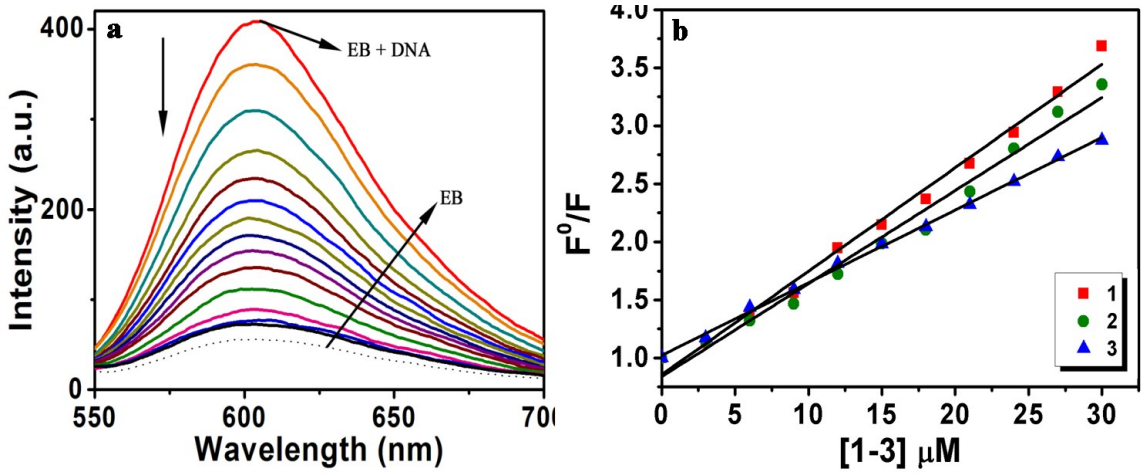

Fig. 3. Emission spectra from EB bound to the DNA in the absence (---) and in the presence of **1** (a). [EB] = 3.3 μM, [DNA] = 3.3 μM, [**1**] = 0-30 μM. Arrow shows changes in the emission intensity upon addition of increasing complex concentration. Stern-Volmer plots of the EB-DNA fluorescence titration for complexes **1**-**3** (b).

Further, the apparent DNA binding constants can also be used to evaluate the three main DNA-binding modes; a value above 10^6 M^{-1} is an indication of intercalation (for example, EB and daunomycin), while values in the range of 10^4-10^5 M^{-1} imply the groove binding mode.[32] Thus to rationalize the DNA binding interaction of the complexes **1**-**3**, apparent binding constants (Kapp) were calculated using equation 3:

$$K_{EB}[EB] = K_{app}[complex] \quad (3)$$

where [complex] is the concentration value at 50% reduction in the fluorescence intensity of EB, K_{EB} (1.0×10^7 M^{-1}) is the DNA binding constant of EB, and [EB] is the concentration of EB (3.3 μM). The K_{app} values for **1**-**3** are found to be 5.5×10^6, 3.33×10^6 and 3.00×10^6 M^{-1}, respectively. From the above data, it is clear that **1** replaces EB more effectively than the other complexes, which is in accord with the results obtained from electronic absorption studies. Although the observed K_{app} values for complexes **1**-**3** are lower than the binding constant of the classical intercalators and metallointercalators (10^7 M^{-1}),[33] from the observed quenching and binding parameters we can ascertain a possible intercalative mode of binding of the complexes to DNA.

Quantum Chemical calculations

Geometry optimization of complexes **1**–**3** has been undertaken at the DFT level of theory to obtain equilibrium structures suitable for the molecular docking studies and to reveal the composition and energies of the frontier molecular orbitals (MOs) of the complexes. X-ray structures of **1** and **3** were used as the starting geometries for the optimization procedure. The general structure of the complexes is preserved as a result of the geometry optimization. The calculated structural parameters are in good agreement with the experimental X-ray data often falling within 3σ-interval of the experimental data (Table S1, ESI).

The highest doubly occupied MO (HOMO) of the complexes is mostly centered at atoms of the naphthalene moiety of the ligand, whereas the lowest unoccupied MO (LUMO) is strongly delocalized between atoms of the ligands (Figs. 4a-b). The spin density is localized mostly at the Cu atom (0.75 e) with small contributions coming from the donor N(1), N(2),

O(1) and O(3) atoms of the ligands and NO_3^- (up to 0.08 e) reflecting some spin delocalization between Cu and the O and N atoms (Fig. 4c).

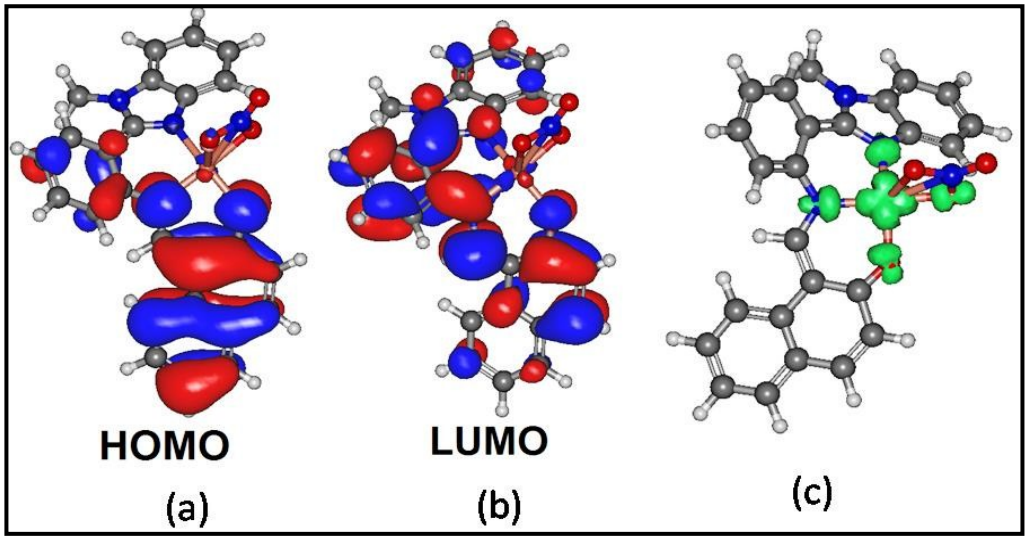

Fig. 4. Plots of the HOMO (a) and LUMO (b) of complex **1**. (c) Calculated spin density distribution in complex **1**.

In the interaction of DNA with complex **1**, the former acts as an electron donor and the latter serves as an electron acceptor. Hence, in terms of the frontier MO theory, such an interaction should be determined by the LUMO energy of the complex. The calculated $LUMO_{complex}$ energies slightly increases from **1** to **3** (–1.59 eV for **1**, –1.55 eV for **2** and –1.54 eV for **3**) correlating with the binding energy estimated by the molecular docking calculations and with the cytotoxicity of complexes (*vide infra*). At the same time, the differences of the LUMO energies is rather small, and other factors may also affect the relative biological activity of these compounds (*e.g.*, electrostatic and van der Waals interactions and steric effects imposed by the varying N-alkyl substituent at the imidazole ring).

Molecular Docking with DNA

The designing of molecules can lead to the recognition of specific sequence and structures of nucleic acids and plays an important role in the development of new chemotherapeutic drugs. Molecular docking studies have played a very significant role in understanding the mechanistic pathway of DNA-drug interactions,[34] by placing a molecule into the binding site of the DNA and delivering the visual representation of the binding of the drugs to DNA, which can substantiate the spectroscopic results. Thus, in order to confirm and rationalize the observed spectroscopic results and to get a further insight into the intercalation ability, the complexes **1**–**3** were successively docked within the DNA duplex of sequence d(CGCGAATTCGCG)$_2$ dodecamer (PDB ID: 1BNA). The resulting docking experiments revealed that the complexes under study interact with B-DNA (PDB ID: 1BNA) to the G-C rich intercalation site[35] of the minor groove (Fig. 5a, **1**; Fig. S17a, **2**; Fig. S18a, **3,** ESI) with relative binding energy of -341.83 (**1**), -302.5 (**2**) and -301.9 (**3**) kJ mol^{-1}. The intercalation ability of these complexes can be due to the presence of the planar naphthalene moiety in the ligand framework which forms π−π staking with the two DNA flanking bases. These interactions are considered to be the main driving force of the intercalation binding mode of the complexes under study and are further stabilized by van der Waals, hydrophobic contacts and hydrogen bonding.[36]

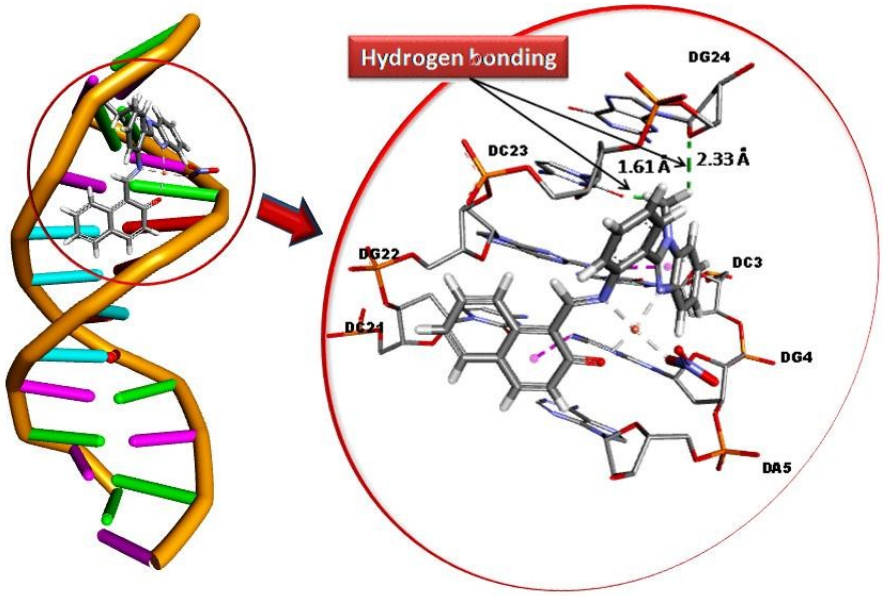

(a) **(b)**

Fig. 5. Molecular docked model of compound **1** with DNA (PDB ID: 1BNA). DG:Guanine, DC: Cytosine, DA: Adenine

To assess the possible role of the N-alkyl moiety in the ligand framework of the complexes in their DNA binding we monitored the hydrogen bonding interaction of the energetically favorable conformation of the docked model for our complexes. For complex **1**, the interaction established two hydrogen bonds involving hydrogen atoms of the N-methyl group and oxygen atom of DG-24 (2.33 Å) and DC-23 (1.61 Å) (Fig. 5b). As for complex **2**, the binding was stabilized by two hydrogen bonds: hydrogen bonding between hydrogen atoms of the N-ethyl group and oxygen atom of DG-24 (2.66 and 2.88 Å) (Fig. S17b, ESI), whereas only one such interaction was observed for **3** involving an hydrogen atom of the N-propyl group and oxygen atom of DG-24 (1.99 Å) (Fig. S18b, ESI). Thus, it can be

concluded that the presence of N-methyl group reinforces the hydrogen bonding between complex **1** and the DNA, consequently stabilizing the system formed by the DNA and this complex, thereby increasing the binding affinity. The greater binding affinity (**1** > **2** > **3**) obtained from molecular docking studies is in agreement with the experimental results acquired from electronic and fluorescence studies.

Cytotoxicity studies

MTT assay

The effectiveness of Schiff base copper(II) complexes to suppress cell growth and promote apoptosis has been well documented.[37] The *in vitro* cell culture studies provide valuable information for the screening of chemotherapeutic agents and preliminary data for further relative studies. Thus, cytotoxicities (IC_{50} values; Table 3; Figs. S19-S21, ESI) of complexes **1**-**3** against three different human cancer cell lines, *viz.* A-549 (lung carcinoma), MDA-MB-231 (breast cancer) and HeLa (cervical cancer) cancer cells, were evaluated through the loss of cell viability using the MTT assay.[19] Complex **1** exhibits a significant inhibitory effect on proliferation of the A-549 cancer cells and is more potent than the widely used drug cisplatin (IC_{50} = 27.2 ± 1.71 μM) under similar experimental condition.[19]

Table 3: IC_{50} values of complexes **1**-**3** against A-549, MDA-MB-231 and HeLa cancer cells (n = 4).

Compounds	Incubation time (24 h)		
	IC_{50} (μM)		
	A-549	MDA-MB-231	HeLa
1	16.7 ± 0.29	29.58 ± 1.17	32.66 ± 0.58
2	24.0 ± 1.99	31.92 ± 0.73	33.79 ± 0.36
3	29.1 ± 1.12	46.03 ± 1.12	45.27 ± 0.65

Further, the IC_{50} values of complex **1** in all the cell lines under study are smaller than those of the related complexes **2** and **3**, suggesting that the N-methyl group of benzimidazole unit renders it more cytotoxic to the cells than the N-ethyl or N-propyl substituents. This is in accord with the DNA binding propensity order of the complexes **1-3**.

Since there are no biological data reported for the benzimidazole Schiff base copper(II) complexes on A-549 cancer cell line, the IC_{50} values of complexes **1-3** have been compared with other related Schiff base copper(II) complexes reported recently (Table 4).[38] The *in vitro* cytotoxicity of our complexes (for A-549) is higher. Moreover, since the *in vitro* cytotoxicity of the complex **1** was found to be the highest one for A-549 among our complexes, all further analysis were carried out using this cell line.

Table 4: Comparison of cytotoxicities [IC_{50} (μM)] of benzimidazole-based copper(II) complexes with related ones.

Compounds	IC_{50} (μM) A-549	Reference
1	16.7 ± 0.29	This paper
2	24.0 ± 1.99	This paper
3	29.1 ± 1.12	This paper
[Cu L_2] [L = (2-Hydroxybenzylidene)isonicotinohydrazide]	475	38a
[Cu L_2] [L = (4-Hydroxy-3-methoxybenzylidene)-N-methylisonicotinohydrazide)]	92	38a
[CuL_2] [L = (4-Methoxybenzylidene)-N-methylisonicotinohydrazide)]	<50	38a
[CuL_2] [L = 2-(((4-phenoxyphenyl)imino)methyl)phenol]	>50	38b
[CuLCl].CH_3OH [L = {2-ethyl-2-((2-hydroxybenzylideneamino)}propane-1,3-diol)]	>50	38c

Nuclear Morphology using Fluorescence Microscope

Chromatin condensation and fragmentation of nucleus is one of the major properties of apoptotic cell death. Thus, to determine the type of cell death (apoptosis or necrosis) caused by complex **1** in A-549 cell line**,** DNA binding dyes, Hoechst 33342/propidium iodide (PI) were used (Fig. 6). In control cells, a uniform level of blue fluorescence nucleus was seen which indicates that almost all cells are alive and healthy. However, for treated cells, early apoptotic cells with deep blue fluorescence (yellow circle), late apoptotic cells with fragmented nucleus (blue circle) and necrotic cells with red fluorescence (red circle) were clearly observed upon increasing concentration of the drug administration (15 and 18 μM). These results clearly suggest that the complex under investigation favors the apoptotic mode of cell death in lung cancer (A-549) cells.

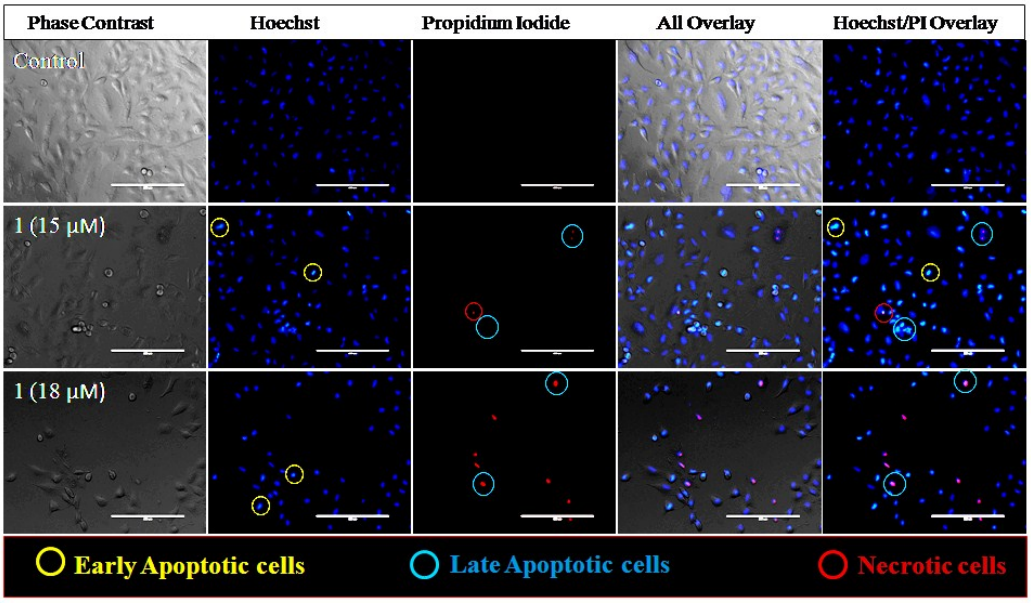

Fig. 6. Images showing morphological changes of complex **1** in lung cancer A-549 cells detected with dual staining of Hoechst 33342/PI. Yellow circle indicates early apoptotic cells, blue circle indicates late apoptotic cells and red circle indicates necrotic cells.

Cell cycle analysis by flow cytometry

Cell cycle is frequently deregulated in cancer diseases and regulation of cell cycle can be an important factor for cure and improvement of patient life. Based on the antiproliferative activity of the complexes **1-3**, complex **1** was chosen for further investigation into the cell death and cell cycle delay on the basis of DNA content in A-549 cells by the fluorescence activated cell sorting (FACS) method using PI staining (Fig. 7). Cells were treated near to the IC_{50} value of complex **1**. According to FACS histogram statistics, the percentage of sub-G1 (apoptotic cell death) cells slightly increased from 1% to 5% in treated group as compared to control. Upon increasing the concentration of complex **1** (10-21 μM), a significant increase from 13% to 30% was observed in G2/M phase of cell cycle, a decrease from 76% to 52% was observed in G1 phase, whereas S phase was found to be almost stable in control and treated group under identical conditions. Histogram statistics of FACS of complex **1** clearly indicate inducing the cell cycle arrest at the G2/M phase and demonstrate a dose-dependent inhibition behavior on the cell proliferation.

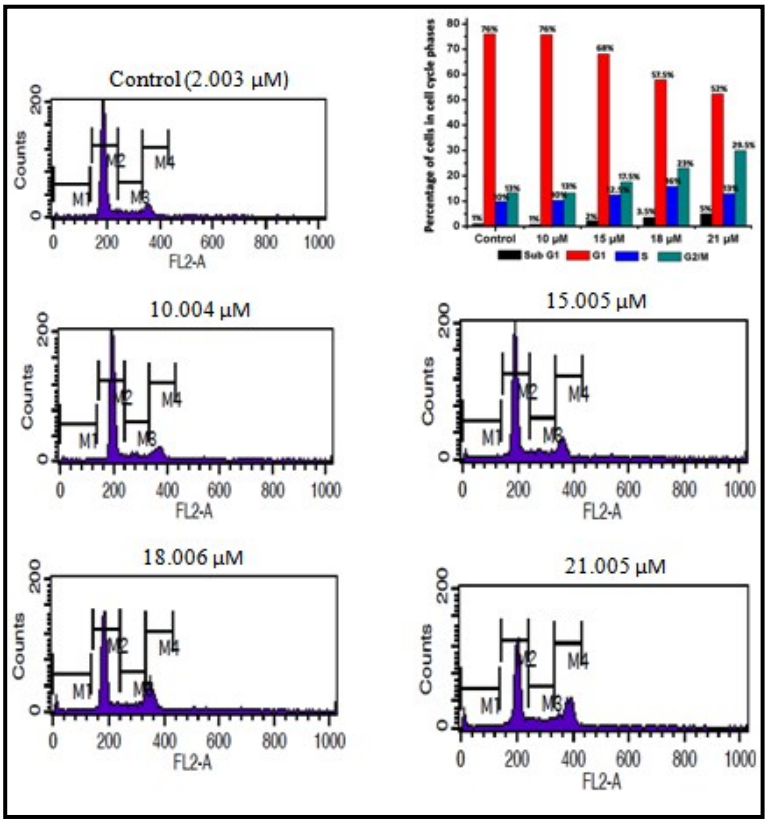

Fig. 7. Distribution of cell cycle phases through FACS analysis of PI-stained A-549 lung cancer cells after 24 h incubation for control and treated groups.

DNA fragmentation assay

To gain further information about the apoptotic cell death induced by complex **1**, apoptotic DNA fragmentation assays have been performed. For this purpose, we have tested three different concentrations of complex **1** (15, 18 and 21 μM) for DNA gel electrophoretic assay and DNA ladder patterns were observed (Fig. 8). As the cell undergoes apoptosis, endonucleases cleave the internucleosomal linker DNA and results in fragmentation of the genome.[39] The fragmented genome gives a laddering pattern on running the gel which is a characteristic feature of apoptosis.[40] As shown in Fig. 8, control DNA do not have any detectable ladder pattern, whereas the introduction of complex **1** (15 μM) caused a remarkable appearance of DNA fragmentation/ladder pattern. This effect becomes more prominent at higher concentrations 18 and 21 μM (lanes 4 and 5, respectively), which is comparable to etoposide, a known DNA damaging agent.[41] These results suggest an apoptotic cell death induced by complex **1** and further supports our hypothesis regarding the antitumor activity.

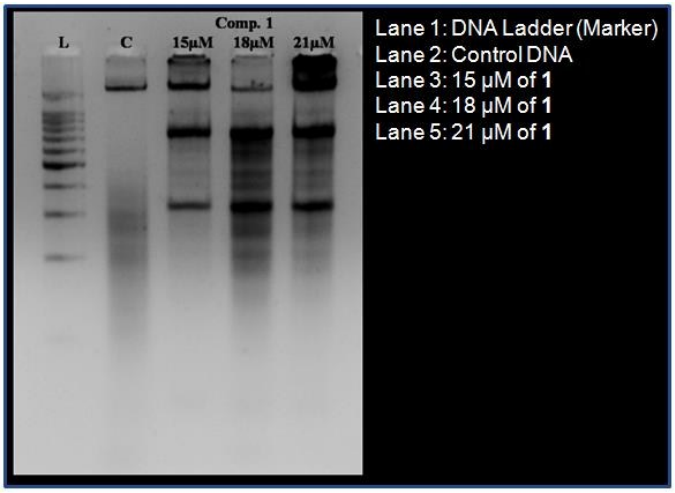

Fig. 8. Images of fragmented DNA of control and treated A-549 cells after electrophoresis in 1.8% agarose gel.

ROS (reactive oxygen species) production in A-549 cells

Copper(II) complexes are known to induce apoptosis by increasing intracellular reactive oxygen species (ROS) level.[42] Intracellular ROS generation for complex **1** at the concentration of 0, 15, 18 and 21 μM, was conducted in A-549 lung cancer cell line by using the DCFH-DA dye in treated as well as in control cells to monitor this effect. As shown in Fig. 9, after 24 h treatment, the complex under study induces an elevated level of ROS generation in a dose dependent manner. These results demonstrate that complex **1** may induce apoptotic pathways mediated by ROS.

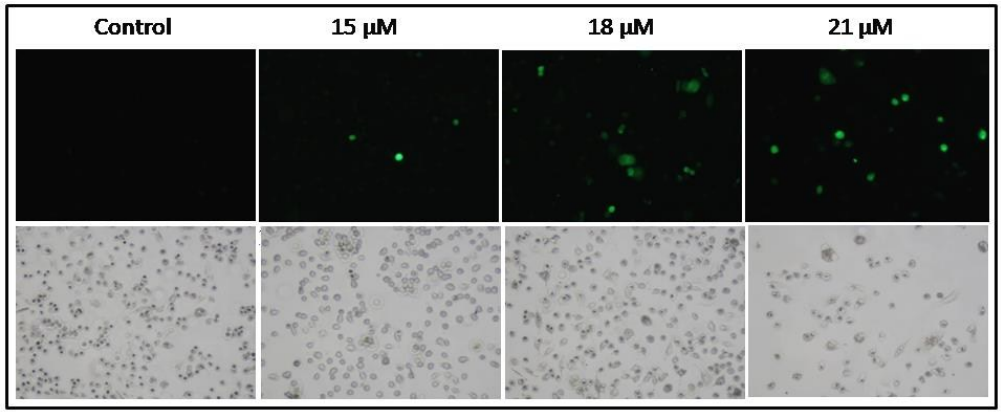

Fig. 9. Generation of ROS induced by **1** in A-549 lung cancer cells.

Conclusions

In conclusion, through the present work new N-alkyl substituted benzimidazole-based Schiff base copper(II) complexes (**1**-**3**) have been described. Various physicochemical techniques demonstrated that these complexes effectively bind to DNA through intercalative mode, in the order of **1** > **2** > **3**. Binding of the complexes to DNA minor groove through intercalative mode has been rationalized by molecular docking studies and provided a deep insight towards the mechanism of interactions with DNA.

The complexes exhibit *in vitro* cytotoxic activity against lung (A-549), breast (MDA-MB-231) and cervical (HeLa) cancer cell lines, with potency of **1** (with the shortest alkyl substituent, i.e., methyl) being even higher than that of the widely used drug cisplatin (IC_{50} = 27.2 ± 1.71 µM) against lung cancer (A-549) cell line. The relatively stronger binding affinity of complex **1** to DNA and *in vitro* cytotoxic activity are thought to be due to the presence of the least bulky N-alkyl moiety in the ligand framework, thus progressively

decreasing with the size increase in the N-alkyl substituent. This is supported by the LUMO energy of the complexes, obtained from quantum chemical calculations which slightly increase from **1** to **3.** The greater antiproliferative activity of the complex **1** was further proved by morphologic, cell cycle, DNA fragmentation and ROS studies. Complex **1** can not only inhibit the proliferation of cancer cell line, but also induces apoptosis.

The benzimidazole derived copper(II) complexes presented herein (in particular **1**) exhibit a considerable biological activity and the studies can contribute to the rational design of novel potential anticancer agents.

Acknowledgements

This work has been partially supported by the Fundação para a Ciência e a Tecnologia (FCT), Portugal, and its UID/QUI/00100/2013 project. The authors A. P. and S. A. are grateful to the FCT for the award of a postdoctoral fellowship (ref: SFRH/BPD/88450/2012 and SFRH/BPD/76451/2011). The authors also acknowledge the Portuguese NMR Network (IST-UL Centre) for access to the NMR facility, and the IST Node of the Portuguese Network of mass-spectrometry (Dr. Conceição Oliveira) for the ESI-MS measurements. B.K. and G.S. acknowledge Interdisciplinary School of Life Sciences (ISLS), Banaras Hindu University, for access to FACs facility.

Supporting Information

Electronic Supplementary Information (ESI) available: CCDC deposition Nos. CCDC 1406556-1406557, experimental procedures, synthesis and characterization, Figs. S1-S14

containing IR, ^{1}H and ^{13}C NMR, ESI-MS, UV/vis, fluorescence, docking materials and Table S1-S2.

References

1 R. A. Alderden, M. D. Hall and T. W. Hambley, *J. Chem. Educ.*, 2006, **83**, 728.

2 (a) X. Wang and Z. Guo, *Chem. Soc. Rev.,* 2013, **42**, 202; (b) J. S Butler and P. J. Sadler, *Curr. Opin. Chem. Biol.*, 2013, **17**, 175; (c) L. Kelland, *Nat. Rev. Cancer,* 2007*,* **7**, 573; (d) D. Wang and S. J. Lippard*, Nat. Rev. Drug Discovery,* 2005*,* **4**, 307.

3 (a) Y. W. Jung and S. J. Lippard, *Chem. Rev.*, 2007, **107**, 1387; (b) T. Boulikas and M. Vougiouka, *Oncol. Rep.*, 2003, **10**, 1663; (c) S. M. Cohen and S. J. Lippard, *Nucleic Acids Res. Mol. Biol.*, 2001, **67**, 93; (d) E. Wong and C. M. Giandomenico, *Chem. Rev.*, 1999, **99**, 2451; (e) A. H. Calvert, D. R. Newell and M. J. Tilby, Cisplatin Nephrotoxicity, Oxford Textbook of Oncology, Oxford University Press, Oxford, New York, 1995, vol 1, p. 552; (f) L. R. Kelland, *Crit. Rev. Oncol. Hematol.*, 1993, **15**, 191; (g) G. Daugaard and U. Abildgaard, Cisplatin nephrotoxicity, *Cancer Chemother. Pharmacol.*, 1989, **25**, 1.

4 (a) C. Santini, M. Pellei, V. Gandin, M. Porchia, F. Tisato and C. Marzano, *Chem. Rev.*, 2014, **114**, 815; (b) A. N. Kate, A. A. Kumbhar, A. A. Khan, P. V. Joshi and V. G. Puranik, *Bioconjugate Chem.*, 2014, **25**, 102; (c) M. A. Cater, H. B. Pearson, K. Wolyniec, P. Klaver, M. Bilandzic, B. M. Paterson, A. I. Bush, P. O. Humbert, S. L. Fontaine, P. S. Donnelly and Y. Haupt, *ACS Chem. Biol.*, 2013, **8**, 1621; (d) D. Gaynora and D. M. Griffith, *Dalton Trans.*, 2012, **41** , 13239; (e) Gao E, Liu C, Zhu M, Lin H, Wu

Q and Liu L, *Anticancer Agents Med Chem.*, 2009, **9**, 356; (f) S. Tardito and L. Marchio, *Curr. Med. Chem.*, 2009, **16**, 1325; (g) X. Zhang, C. Bi, Y. Fan, Q. Cui, D. Chen, Y. Xiao and Q. Ping Dou, *Int. J. Mol. Med.*, 2008, **22**, 677; (h) J. M. Rademaker-Lakhai, D. Van den Bongard, D. Pluim, J. H. Beijnen and J. H. Schellens, *Clin. Cancer Res.*, 2004, **10**, 3717; (i) T. Theophanides and J. Anastassopoulou, *Crit. Rev. Oncol. Hematol.*, 2002, **42**, 57; (j) G. J. Brewer, *Exp. Biol. Med.*, 2001, **226**, 665; (k) J. K. Barton, in Bioinorganic Chemistry, ed. I. Bertini, H. B. Grey, S. J. Lippard and J. S. Valentine, University Science Book, Mill Valley, 1994, p. 455.

5 (a) S. Tabassum, M. Ahmad, M. Afzal, M. Zaki and P. K. Bharadwaj, *J. Photochem. Photobio. B: Bio.,* 2014, **114**, 321; (b) L. Finney, S. Vogt, T. Fukai and D. Glesne, *Clin. Exp. Pharmacol. Physiol.*, 2009, **36**, 88.

6 Y.-F. Li and Z. -Q. Liu, *Eur. J. Pharm. Sci.*, 2011, **44**, 158.

7 (a) A. A. Holder, P. Taylor, A. R. Magnusen, E. T. Moffett, K. Meyer, Y. Hong, S. E. Ramsdale, M. Gordon, J. Stubbs, L. A. Seymour, D. Acharya, R.T. Weber, P. F. Smith, G. C. Dismukes, P. Ji, L. Menocal, F. Bai, J. L. Williams, D.M. Cropek and W.L. Jarrett, *Dalton Trans.*, 2013, **42**, 11881; (b) M. X. Li, L. Z. Zhang, C. L. Chen, J. Y. Niu, B. S. Ji, *J. Inorg. Biochem.*, 2012, **106**, 117; (c) Z.-Y. Ma, X. Qiao, C. -Z. Xie, J. Shao, J.-Y. Xu, Z.-Y. Qiang, J.-S. Lou, *J. Inorg. Biochem.*, 2012, **117**, 1; (d) L. -X. Cheng, J. -J. Tang, H. Luo, X. -L. Jin, F. Dai, J. Yang, Y. -P. Qian, X. -Z. Li and B. Zhou, *Bioorg. Med. Chem. Lett.*, 2010, **20**, 2417; (e) P.U. Maheswari, S. Roy, H. den. Dulk, S. Barends, G. van Wezel, B. Kozlevcar, P. Gamez, J. Reedijk, *J. Am. Chem. Soc.*, 2006, **128**, 710; (f) N. Farrell, *Coord. Chem. Rev.*, 2002, **232**, 1.

8 (a) J. Pragathi, K. Mounika, M. Padmaja, M. Lakshmi, C. Gyanakumari, *Eur. J. Chem.,* 2011, **8**, , 1662; (b) H. Marijana, S. Kristina, K. Sandra, *Eur. J. Med. Chem.*, 2011, **46**, 2274; (c) Y. S. Chhonker, B. Veenu, S.R. Hasim, *Eur. J. Chem.*, 2009, **6**, S342.

9 (a) U. C. Saha, B. Chattopadhyay, K. Dhara, S. K. Mandal, S. Sarkar, ^ A. R. Khuda-Bukhsh, M. Mukherjee, M. Helliwell and P. Chattopadhyay, *Inorg. Chem.*, 2011, **50**, 1213; (b) R. Pandey, R. K. Gupta, M. Shahid, B. Maiti, A. Misra and D. S. Pandey, *Inorg. Chem.*, 2012, **51**, 298; (c) S. Mukhopadhyaya, R. K. Gupta, A. Biswas, A. Kumar, M. Dubey, M. S. Hundal and D. S. Pandey, *Dalton Trans.*, 2015, **44**, 7118.

10 (a) L. Arzuman, P. Beale, C. Chan, J Q. Yu and F. Huq, *Anticancer Res.*, 2014, **34**, 5453; (b) N. T. Abdel Ghani and A. M. Mansour, *Eur. J. Med. Chem.*, 2012, **47**, 399; (c) N. T. Abdel Ghani and A. M. Mansour, *Spectrochim. Acta Part A*, 2011, **81**, 529; (d) N. T. Abdel Ghani and A. M. Mansour, *J. Mol. Struct.*, 2011, **991**, 108; (e) F. Gumus, I. Pamuk, T. Ozden, S. Yıldız, N. Diril, E. Oksuzoglu, S. Gur and A. Ozkul, *J. Inorg. Biochem*., 2003, **94**, 255; (f) F. Gumus, O. Algul, G. Eren, H. Eroglu, N. Diril, S. Gur and A. Ozkul, *Eur. J. Med. Chem*., 2003, **38**, 473; (g) F. Gumus, A. B. Ozcelik, T. Ozden, H. Eroglu and N. Diril, *Pharmazie* 2003, **58**, 303; (h) F. Gumus and O. Algul, *J. Inorg. Biochem*., 1997, **68**, 71.

11 (a) P. Tyagi, S. Chandra, B. S. Saraswat and D. Sharma, *Spectrochim. Acta A. Mol. Biomol. Spectrosc.*, 2015, **143**, 1; (b) A. Paul, R. K. Gupta, M. Dubey, G. Sharma, B. Koch, G. Hundal, M. S. Hundal and D. S. Pandey, *RSC Adv.*, 2014, **4**, 41228; (c) W. Song , J.-P. Cheng , D.-H. Jiang , L Guo, M.-F. Cai, H.-B. Yang, Q.-Y. Lin, *Spectrochim. Acta A. Mol. Biomol. Spectrosc.*, 2014, **121**, 70.

12 F. Gumus¸ G. Eren, L. Acık, A. Celebi, F. Ozturk, S.Yılmaz, R. I. Sagkan, S. Gur, A. Ozkul, A. Elmalı and Y. Elerman, *J. Med. Chem.,* 2009**, 52**, 1345.

13 D. D. Perrin, W. L. F. Armarego and D. R. Perrin, Purification of Laboratory Chemicals; Pergamon Press: Oxford, 1980.

14 (a) Bruker, APEX2 & SAINT, AXS Inc., Madison, WI, 2004; (b) A. Altomare, M. C. Burla, M. Camalli, G. L. Cascarano, C. Giacovazzo, A. Guagliardi, A. G. G. Moliterni, G. Polidori, R. Spagna, *J. Appl. Cryst.* 1999, **32**, 115; (c) G. M. Sheldrick, *Acta Cryst.*, 2008, **A64**, 112; (d) L. J. Farrugia*, J. Appl. Cryst*., 1999, **32**, 837.

15 S. Anbu, A. Paul, R. Ravishankaran, M. F. C. Guedes da Silva, A. A. Karande, A. J.L. Pombeiro, *Inorg. Chim. Acta*, 2014, **423**, 183.

16 Y. Zhao, D. G. Truhlar, *Theor. Chem. Acc.,* 2008, **120**, 215.

17 (a) M. J. Frisch, G. W. Trucks, H. B. Schlegel, G. E. Scuseria, M. A. Robb, J. R. Cheeseman, G. Scalmani, V. Barone, B. Mennucci, G. A. Petersson, H. Nakatsuji, M. Caricato, X. Li, H. P. Hratchian, A. F. Izmaylov, J. Bloino, G. Zheng, J. L. Sonnenberg, M. Hada, M. Ehara, K. Toyota, R. Fukuda, J. Hasegawa, M. Ishida, T. Nakajima, Y. Honda, O. Kitao, H. Nakai, T. Vreven, Jr., J. A. Montgomery, J. E. Peralta, F. Ogliaro, M. Bearpark, J. J. Heyd, E. Brothers, K. N. Kudin, V. N. Staroverov, R. Kobayashi, J. Normand, K. Raghavachari, A. Rendell, J. C. Burant, S. S. Iyengar, J. Tomasi, M. Cossi, N. Rega, J. M. Millam, M. Klene, J. E. Knox, J. B. Cross, V. Bakken, C. Adamo, J. Jaramillo, R. Gomperts, R. E. Stratmann, O. Yazyev, A. J. Austin, R. Cammi, C. Pomelli, J. W. Ochterski, R. L. Martin, K. Morokuma, V. G. Zakrzewski, G. A. Voth, P. Salvador, J. J. Dannenberg, S. Dapprich, A. D. Daniels, O. Farkas, J. B. Foresman, J. V. Ortiz, J.

Cioslowski and D. J. Fox, *Gaussian 09*, Revision A.01, Gaussian, Inc., Wallingford CT, 2009.

18 M. Dolg, U. Wedig, H. Stoll and H. Preuss, *J. Chem. Phys.,* 1987, **86**, 866.

19 T. J. Mosmann, *J. Immunol. Methods,* 1983, **65**, 55.

20 P. L. Kuo, Y. L. Hsu, C. H. Chang and C. C. Lin, *Cancer Lett.,* 2005, **223**, 293.

21 (a) K. Nakamoto, Infrared and Raman Spectra of Inorganic and Coordination Compounds, Part B. Applications in Coordination, Organometallic, and Bioinorganic Chemistry, Wiley-Interscience, Hoboken, 2009. (b) S. Anbu, R. Ravishankaran, M. F. C. Guedes da Silva, A. A. Karande, and A. J. L. Pombeiro, *Inorg. Chem*., 2014, **53**, 6655.

22 M. Hazra,T. Dolai, A. Pandey, S. K. Dey and A. Patra, Bioinorganic Chemistry and Applications, Volume 2014, Article ID 104046.

23 A. W. Addison, T. N. Rao, J. Reedijk, G. C. Verschoor, *J. Chem. Soc. Dalton Trans.,* 1984, 1349.

24 (a) A. F. Tanious, D. Y. Ding, D. A. Patrick, C. Bailly, R. R. Tidwell and W. D. Wilson, *Biochemistry,* 2000, **39**, 12091; (b) C. Y. Zhong, J. Zhao, Y. B. Wu, C. X. Yin and P. *J*. Yang, *Inorg. Biochem.,* 2007, **101**, 10.

25 M. Baldini, M. Belicchi-Ferrari, F. Bisceglie, P. P. Dall'Aglio, G. Pelosi, S. Pinelli and P. Tarasconi, *Inorg. Chem.,* 2004, **43**, 7170.

26 (a) Carter, M. T.; Rodriguez, M.; Bard, A. J. *J*. *Am*. *Chem*. *Soc*., 1989, **111**, 8901; (b) Mcghee, J. D.; Hippel, P. H. V. *J*. *Mol*. *Biol*., 1974, **86**, 469; (c) Nelson, D. L.; Cox, M. M. *Lehninger Principles of Biochemistry*, W. H. Freeman and Company, New York, 4th edn, 2005, p. 516.

27 S. Anbu, M. Kandaswamy, P. Suthakaran, V. Murugan and B. Varghese, *J. Inorg. Biochem.*, 2009, **103**, 401.

28 (a) X. B. Fu, Z. H. Lin, H. F. Liu, X. Y. Le, *Spectrochim. Acta Mol. Biomol. Spectrosc.*, 2014, **122**, 22; (b) H. Wu, F. Kou, F. Jia, B. Liu, J. Yuan and Y. Bai, *Bioinorg. Chem. Appl.*, 2011, Article ID 105431.

29 D. L. Boger, S. R. Fink, S. R. Brunette, W. C. Tse and M. P. Hedrick, *J. Am. Chem. Soc.*, 2001, **123**, 5878.

30 (a) S. Anbu, M. Kandaswamy and B. Varghese, *Dalton Trans.*, 2010, **39**, 3823; (b) L. Leelavathy, S. Anbu, M. Kandaswamy, N. Karthikeyan, N. Mohan, *Polyhedron*, 2009, **28**, 903; (c) S. Anbu, S. Kamalraj, B. Varghese, J. Muthumary, M. Kandaswamy. *Inorg. Chem.*, 2012, **51**, 5580.

31 D. Herebian and W. S. Sheldrick, *J. Chem. Soc., Dalton Trans.,* 2002, 966.

32 X. Sheng, X. M. Lu, Y. T. Chen, G. Y. Luo, J. J. Zhang, Y. Shao, F. Liu and Q. Xu, *Chem. - Eur. J.,* 2007, **13**, 9703.

33 M. Cory, D. D. McKee, J. Kagan, D. W. Henry and J. A. Miller, *J. Am. Chem. Soc.,* 1985, **107**, 2528.

34 (a) Y. Gilad and H. Senderowitz, *J. Chem. Inf. Model.*, 2014, **54**, 96; (b) N. Minovski, A. Perdih, M. Novic, and T. Solmajer, *J. Comput. Chem.*, 2013, **34**, 790.

35 D. R. Boer, A. Canals and M. Coll, *Dalton Trans.*, 2009, 399.

36 (a) M. Baginski, F. Fogolari and J. M. Briggs, *J. Mol. Biol.* 1997, **274**, 253; (b) C. Rehn and U. Pindur, *Monatsh. Chem.,* 1996, **127**, 631; (c) M. J. Waring and C. Bailly, *Gene*, 1994, **149**, 69.

37 (a) S. Roy, P. U. Maheswari, M. Lutz, A. L. Spek, H. den Dulk, S. Barends, G. P. van Wezel, F. Hartl and J. Reedijk, *Dalton Trans.*, 2009, 10846; (b) S. Gama, F. Mendes, F. Marques, I. C. Santos, M. F. Carvalho, I. Correia, J. C. Pessoa, I. Santos and A. Paulo, *J. Inorg. Biochem.*, 2011, **105**, 637; (c) Z.-C. Liu, B. D. Wang, B. Li, Q. Wang, Z.-Y. Yang, T. R. Li and Y. Li, *Eur. J. Med. Chem*., 2010, **45**, 5353; (d) D. S. Raja, N. S. P. Bhuvanesh and K. Natarajan, *Inorg. Chem.*, 2011, **50**, 12852.

38 (a) P. Ramadevi, R. Singh, A. Prajapati, S. Gupta and D. Chakraborty, *Advances in Chemistry*, 2014, Article ID 630575; (b) M. Niu, M. Hong, G. Chang, X. Li and Z. Li, *J. Photochem. Photobiol., B*, 2015, **148**, 232; (c) M. Niu, Z. Li, H. Li, X. Li, J. Dou and S. Wang, *RSC Adv.*, 2015, **5**, 37085.

39 A. H. Wyllie, *Nature*, 1980, **284**, 555.

40 D. R. Linfert, C. Chen, L. Ma, T. Lai and G. J. Tsongalis, *Clin. Chem.*, 1997, **43**, 2431.

41 A. R. Tee and C. G. Proud, *Oncogene*, 2000, **19**, 3021.

42 (a) J. Shaoa, Z. Maa, A. Li, Y. H. Liu, C. Z. Xie, Z. Y. Qiang and J. Y. Xu, *J. Inorg. Biochem*., 2014, **136**, 13; (b) W. Guo, S. Ye, N. Cao, J. Huang, J. Gao and Q. Chen, *Exp. Toxicol. Pathol*., 2010, **62**, 577; (c) L. E. Bröker, F. A. Kruyt and G. Giaccone, *Clin. Cancer Res*., 2005, **11**, 3155.

Table 1. Crystal data and structure refinement parameters for **3.**

	1	**3**

Empirical formula	$C_{25}H_{18}CuN_4O_4$	$C_{27}H_{22}CuN_4O_4$
Crystal system	orthorhombic	triclinic
Space group	*P*bca	*P*-1
a (Å)	14.9763(5)	9.9413(7)
b (Å)	10.5573(3)	15.3917(10)
c (Å)	27.4132(11)	17.7468(11)
β (deg)	90	85.698(5)
V (Å^3), *Z*	4334.3(3), 8	2419.9(3), 4
λ (Å)	0.71073	0.71069
Colour and habit	green, block	green, needle
T (K)	296(2)	296(2)
Reflns collected	91187	31610
Refins obs / unique	4136/2728	8595/5497
D_{calcd} (Mg m^{-3})	1.539	1.455
μ (mm^{-1})	1.050	0.944
GOF on F^2	1.012	1.050
R_{int}	0.0337	0.0650
final *R* indices *I*>2σ(*I*)	R1 = 0.0424	R1 = 0.1020
	wR2 = 0.0928	wR2 = 0.2552
R indices (all data)	R1 = 0.0824	R1 = 0.1497
	wR2 = 0.1112	wR2 = 0.2796

Table 2: Selected bond distances (Å) and angles (º) for compounds **1** and **3**.

	1	**3**
Cu–N	1.939(3) 1.944(2)	1.926(6) 1.927(6) 1.973(6) 1.980(6)
Cu–O_L	1.868(2)	1.862(5)
Cu–$O_{nitrate}$	2.023(2) 2.433(3)	1.990(6) 2.021(6) 2.455(9) 2.497(7)
N–Cu–O_L	157.96(11)	158.9(3) 140.8(2)
Largest N–Cu–$O_{nitrate}$	163.91(12)	165.0(3) 159.5(3)
N–Cu–N	91.95(10)	91.2(3) 93.1(2)